Article

Discovery Medicine 2026; 38(214): 3587–3599
https://doi.org/10.24976/Discov.Med.202638214.273

NIMA-Related Kinase 7 Suppresses Proliferation and Invasion of Non-Small Cell Lung Cancer Cells and is Associated With NLRP3 Inflammasome-Related Pyroptotic Signaling

Qiuyan Lin[1], Shaofei Yuan[1], Xiaoqiang Chen[1], Linjia Zhu[2,*]

[1]Department of Oncology, The Third Affiliated Hospital of Wenzhou Medical University, 325200 Wenzhou, Zhejiang, China
[2]Department of Respiratory Medicine, The Third Affiliated Hospital of Wenzhou Medical University, 325200 Wenzhou, Zhejiang, China
*Correspondence: linjia8343@163.com (Linjia Zhu)
Submitted: 22 June 2026 Revised: 9 September 2026 Accepted: 28 September 2026 Published: 25 November 2026

Background: Lung cancer continues to impose a substantial global disease burden because of its high incidence and mortality. On this basis, we investigated the expression pattern of NIMA-related kinase 7 (NEK7) in non-small cell lung cancer (NSCLC) and assessed the biological consequences of altering NEK7 levels, with particular attention to cell growth, invasiveness, metastatic traits, and pyroptosis. We further investigated whether the NLRP3-mediated pyroptosis pathway is involved in these processes.
Methods: Publicly available lung adenocarcinoma (LUAD) and lung squamous cell carcinoma (LUSC) data from UALCAN were first interrogated to characterize the expression pattern of NEK7. Its transcript and protein expression was subsequently validated across lung epithelial and NSCLC cell lines using quantitative real-time polymerase chain reaction (qRT-PCR) and immunoblotting, respectively. Based on these expression profiles, A549 and H1703 cells were chosen for functional experiments in which NEK7 levels were experimentally increased or reduced. Changes in clonogenic growth and invasive behavior were assessed using colony-forming and Matrigel-based chamber assays, respectively. Then, a series of assays were performed to examine changes in pyroptosis. Gasdermin D (GSDMD) fluorescence intensity was observed using immunofluorescence, the expression of various inflammasome-related proteins was detected using Western blotting, and the levels of interleukin (IL)-1β and IL-18 released by the cells were measured with enzyme-linked immunosorbent assay (ELISA) kits. These results were considered together to evaluate pyroptosis-related changes.
Results: Analysis of clinical tissue samples showed that NEK7 expression was significantly lower in non-small cell lung cancer tissues than in normal lung tissues ($p < 0.05$). In the cell-based functional experiments, reducing NEK7 expression in A549 and H1703 lung cancer cells markedly enhanced cell growth, proliferation, and invasive capacity. In contrast, forced upregulation of NEK7 effectively suppressed the proliferative and invasive abilities of these lung cancer cells, with all differences reaching statistical significance (all $p < 0.05$). In addition, NEK7 overexpression was associated with increased GSDMD fluorescence intensity and enhanced expression of inflammasome-related proteins, together with increased interleukin-1β and interleukin-18 levels (all $p < 0.05$). The NLRP3 inhibitor MCC950 partially reversed the inhibitory effect of NEK7 overexpression on cell function ($p < 0.05$), suggesting that NLRP3-related signaling may be involved in the changes in the malignant phenotype associated with NEK7 overexpression in NSCLC cells.
Conclusions: NEK7 is downregulated in NSCLC, and increased NEK7 expression is associated with reduced proliferation and invasion of NSCLC cells *in vitro*. The results of this study suggest that NLRP3-associated pyroptotic signaling may be involved in the biological effects of NEK7 in lung cancer cells. These findings provide a new reference for further elucidating the biological role of NEK7 in non-small cell lung cancer.

Keywords: NIMA-related kinase 7; nod-like receptor protein 3; pyroptosis; NSCLC

Introduction

The global burden of lung cancer remains substantial, with persistently high numbers of new cases and deaths. In clinical practice, more than 80% of lung cancers are classified as non-small cell lung cancer (NSCLC), which mainly includes lung adenocarcinoma, lung squamous cell carcinoma, and large cell carcinoma, with lung adenocarcinoma and lung squamous cell carcinoma being the most common types [1,2]. One of the major challenges in the management of this cancer is that early-stage disease is often present with nonspecific symptoms, resulting in delayed recognition. By the time it is detected, many patients have already progressed to the intermediate or advanced stage. As the disease progresses, it can not only damage normal lung function but also easily spread throughout the

Copyright: © 2026 The Author(s). Published by Discovery Medicine. This is an open access article under the CC BY 4.0 license.
Note: *Discovery Medicine* stays neutral with regard to jurisdictional claims in published maps and institutional affiliations.

body, adversely affecting patients' quality of life and even directly leading to death [3]. However, cancer research has advanced rapidly in recent years, and new treatment approaches, such as targeted therapy and immunotherapy, have gradually been introduced into clinical practice, providing new treatment options for patients with this type of lung cancer [4,5].

Pyroptosis is a form of regulated cell death accompanied by an inflammatory response [6]. It is characterized by disruption of the cell membrane and the release of intracellular inflammatory factors into the extracellular space [7]. Pyroptosis has been implicated in the development of various tumors, including gastrointestinal tumors and cervical cancer [8]. The NLRP3 inflammasome is a key complex that triggers pyroptosis and is mainly composed of NLRP3, Apoptosis-associated speck-like protein containing a CARD (ASC), and Caspase-1 [9]. When cells are exposed to external stress or stimuli, the inflammasome assembles and becomes activated, thereby activating downstream Caspase-1. Activated Caspase-1 cleaves GSDMD, allowing it to form pores in the cell membrane and ultimately leading to cell lysis and death. At the same time, Caspase-1 can also activate inflammatory factors such as interleukin (IL)-1β and IL-18, leading to their abundant release and aggravating local inflammation [10,11]. NLRP3 dysregulation has been implicated in tumor growth, progression, metastasis, and patient prognosis [12]. Moreover, the role of NLRP3 is not fixed and can vary according to tumor type and the tumor microenvironment. For example, in breast cancer, pyroptosis triggered by NLRP3 activation can suppress tumor progression and metastasis [13]. In colon cancer, loss of NLRP3 markedly weakens pyroptosis, whereas restoration of NLRP3 expression can restore the antitumor effects of pyroptosis [14]. NLRP3 has also been implicated in the progression of lung cancer [15]. Once activated, this pathway can promote the secretion of inflammatory factors and further contribute to tumor growth, neovascularization, invasion, metastasis, and immune evasion [15]. However, the specific way in which the NLRP3 pathway operates in NSCLC and affects disease progression has not yet been fully clarified.

NEK7 is a protein kinase that was initially recognized mainly for its role in regulating the cell cycle [16]. Subsequent studies have shown that NEK7 acts upstream of the NLRP3 inflammasome and serves as a key role in its activation, thereby directly regulating pyroptosis. NEK7 can bind to the NLRP3 protein and promote inflammasome assembly, thereby initiating pyroptosis [17,18]. However, it is still unclear whether NEK7 expression is increased or decreased in NSCLC, and whether changes in NEK7 expression are associated with the proliferative and invasive abilities of lung cancer cells and NLRP3-related pyroptotic signaling. To address these questions, this study examined NEK7 expression in NSCLC, explored its association with the malignant phenotype of lung cancer cells, and investigated the possible involvement of NLRP3-related pyroptotic signaling.

Materials and Methods

Bioinformatics Analysis

Publicly available RNA-sequencing data for lung adenocarcinoma (LUAD) and lung squamous cell carcinoma (LUSC) were analyzed using the UALCAN database (http://ualcan.path.uab.edu/) [19,20], which integrates level 3 RNA-seq data from The Cancer Genome Atlas (TCGA). *NEK7* mRNA expression was compared between primary tumor tissues and normal lung tissues. The analysis included 515 primary tumor and 59 normal samples for LUAD, and 503 primary tumor and 52 normal samples for LUSC. UALCAN processes TCGA RNA-seq data using RNA-Seq by Expectation Maximization (RSEM)-derived expression estimates and reports gene expression in transcripts per million (TPM) [20]. Expression distributions were generated directly by the UALCAN platform, and differences between normal and primary tumor groups were assessed using Welch's *t*-test according to the statistical procedure implemented in UALCAN [19]. A p value < 0.05 was considered statistically significant. No additional normalization or transformation of the UALCAN-derived results was performed in the present study.

Cell Culture

Lung bronchial epithelial cell line HBE (SNL-646) and NSCLC cell lines, including H1703 (SNL-384), HCC827 (SNL-210), A549 (SNL-089), Calu-1 (SNL-278), and H460 (SNL-088), were purchased from SUNNCELL (Wuhan, China) and identified by short tandem repeat analysis. NLRP3 inhibitor MCC950 (SJ-MX0058A, Jinan, China) was purchased from SparkJade. Cells were cultured at 37 °C with 5% CO_2 in a humidified incubator (Heracell VIOS 160i, Thermo Fisher Scientific, Waltham, MA, USA). The absence of intracellular mycoplasma was confirmed using a mycoplasma detection kit (40612ES25, YEASEN BIO, Shanghai, China).

Quantitative Real-Time Polymerase Chain Reaction (qRT-PCR)

RNA isolation was performed using TRIzol reagent (15596026CN, Invitrogen, San Diego, CA, USA). cDNA synthesis was carried out using the PrimeScript RT Reagent Kit (RR047A, Takara Bio Inc., Kusatsu, Japan). Quantitative amplification was performed using TB Green Premix Ex Taq II (RR820A, Takara Bio Inc., Kusatsu, Japan) in a total reaction volume of 10 µL. Quantitative PCR was performed on a QuantStudio 3 Real-Time PCR System (A28137, Thermo Fisher Scientific, Waltham, MA, USA). *NEK7* was amplified with the forward primer 5′-CACCTGTTCCTCAGTTCCAAC-3′ and the reverse primer 5′-CTCCATCCAAGAGACAGGCTG-

3′. For β-actin (*ACTB*), the forward primer was 5′-CATGTACGTTGCTATCCAGGC-3′, and the reverse primer was 5′-CTCCTTAATGTCACGCACGAT-3′. The NEK7 primers were custom-synthesized by Sangon Biotech (Shanghai, China), and the ACTB primers were obtained from Sangon Biotech (B661202, Shanghai, China). PCR cycling began with an initial denaturation step at 95 °C for 60 s, followed by 40 cycles of denaturation at 95 °C for 5 s and annealing/extension at 60 °C for 20 s. β-actin was used as the reference gene for normalization, and relative *NEK7* mRNA expression was calculated using the $2^{-\Delta\Delta CT}$ method.

Western Blotting (WB)

Protein was extracted from the cell samples using radioimmunoprecipitation assay lysis buffer (RIPA; ab156034, Abcam, Cambridge, UK). Protein concentrations were determined using a BCA protein assay kit (P0011, Beyotime, Shanghai, China). Equal amounts of protein (30 µg per lane) were separated on 10% SDS-PAGE gels and subsequently transferred onto nitrocellulose membranes (E803-01, Vazyme, Nanjing, China). After blocking with TBST (Tris-buffered saline with Tween 20, T1086, Solarbio, Beijing, China) containing 5% skim milk (A600664, Sangon Biotech, Shanghai, China) for 1 h, the membranes were incubated overnight at 4 °C with primary antibodies against NEK7 (ab133514, Abcam, Cambridge, UK; 1:1000), β-actin (4970S, Cell Signaling Technology, Danvers, MA, USA; 1:1000), NLRP3 (15101S, Cell Signaling Technology, Danvers, MA, USA; 1:1000), ASC/TMS1 (13833S, Cell Signaling Technology, Danvers, MA, USA; 1:1000), and Caspase-1 (2225S, Cell Signaling Technology, Danvers, MA, USA; 1:1000). The following day, the membranes were incubated with HRP-linked goat anti-rabbit IgG (ab6721, Abcam, Cambridge, UK; 1:5000) for 1 h. Chemiluminescent signals were developed using an ECL reagent (36208ES60, YEASEN, Shanghai, China). Protein bands were visualized using a ChemiDoc XRS+ imaging system (Bio-Rad, Hercules, CA, USA). Densitometric analysis was performed using ImageJ software (version 1.54f, National Institutes of Health, Bethesda, MD, USA). The relative expression level of each target protein was calculated by dividing the densitometric value of the target protein band by that of the corresponding β-actin band, and the resulting values were normalized to the respective control group.

Transfection

In this experiment, A549 and H1703 cells were divided into four groups: overexpression negative control (OE-NC), NEK7 overexpression (OE-NEK7), knockdown negative control (sh-NC), and NEK7 knockdown (sh-NEK7). Three shRNAs targeting *NEK7* were used: sh-NEK7-1, 5′-CCGGATATGGGCTATAATACATT-3′; sh-NEK7-2, 5′-ACCATCCAAATGTAATAAAATAT-3′; and sh-NEK7-3, 5′-GTCATGCATAGAGATATAAAACC-3′. The sh-NC sequence was 5′-TACTTTCTATCGTGACATAATGA-3′. sh-NEK7 and sh-NC vectors were constructed using GeneChem (Shanghai, China). NEK7 overexpression plasmid containing the full-length coding sequence of human *NEK7* (RefSeq: NM_133494.3) was constructed using the GV230 vector by GeneChem. A549 and H1703 cells were seeded in 6-well plates (BS-06-6, BKMAM, Changde, China) at a density of 2×10^5 cells/well and cultured until approximately 70% confluence. For each well, 2.5 µg of the NEK7 overexpression plasmid, sh-NEK7 plasmid, or corresponding control vector was transfected using 7.5 µL of Lipofectamine 3000 transfection reagent (L3000008, Thermo Fisher Scientific). The transfection complexes were prepared according to the manufacturer's instructions and added to the cells. Cells were cultured for 72 h after transfection before subsequent experiments. All transfections were transient. qRT-PCR and WB analyses were subsequently performed to evaluate transfection efficiency. All groups were handled in parallel under identical transfection and culture conditions to minimize treatment-related variability.

MCC950 Treatment

For the MCC950 intervention experiment, A549 and H1703 cells were divided into the OE-NC, OE-NEK7, and OE-NEK7+MCC950 groups. After 72 h of transfection, MCC950 was added to the OE-NEK7 group at a final concentration of 10 µM and incubated for 8 h before subsequent flow cytometry, colony formation, and Transwell assays.

Cell Colony Formation Experiments

Following transfection, A549 and H1703 cells were seeded into 6-well plates at a density of 1×10^3 cells/well and cultured under standard conditions for 14 days. The culture medium was replaced every 3 days to maintain adequate nutrient supply. At the end of the culture period, the colonies were gently washed with PBS (Phosphate-buffered saline, B310KJ, BasalMedia, Shanghai, China), fixed with 4% paraformaldehyde (158127, Sigma-Aldrich, St. Louis, MO, USA), and stained with 0.05% crystal violet (C0121, Beyotime, Shanghai, China) for 5 min. Colonies containing at least 50 cells were considered valid colonies, and the number of colonies in each well was quantified using ImageJ software.

Transwell Assay

To evaluate the invasive ability of lung cancer cells, 24-well Transwell chambers with 8.0-µm pore polycarbonate membrane inserts (3422, Corning Incorporated, Corning, NY, USA) were used. For the invasion assay, the upper surface of each insert was coated with 30 µL of growth factor-reduced Matrigel (356230, Corning Incorporated) and incubated at 37 °C for 1 h to allow gel forma-

tion. A total of 2.5 × 10^4 cells suspended in 100 µL of serum-free medium were seeded into the upper chamber, while 700 µL of complete medium containing 10% fetal bovine serum (FBS) was added to the lower chamber as a chemoattractant. No exogenous cytokines were added to either chamber. Cells were incubated at 37 °C with 5% CO_2 for 24 h. After incubation, cells that had migrated through the chamber membrane to the lower surface were fixed with 4% paraformaldehyde (P0098, Beyotime, Shanghai, China) and stained with crystal violet. Images were then captured using a CKX53 inverted microscope (Olympus Corporation, Tokyo, Japan), and the number of invaded cells was quantified.

Immunofluorescence Assay

A549 and H1703 cells were fixed with 4% paraformaldehyde for 15 min at room temperature and permeabilized with 0.1% Triton X-100 (A110694, Sangon Biotech, Shanghai, China) for 10 min. After washing with PBS, the cells were blocked with 5% BSA (A600332, Sangon Biotech, Shanghai, China) in PBS for 1 h at room temperature. The cells were then incubated overnight at 4 °C with an anti-GSDMD primary antibody (ab219800, Abcam; 1:50). After washing with PBS, a Cy3-labeled secondary antibody (GB21303, Servicebio, Wuhan, China; 1:1000) was applied for 1 h at room temperature in the dark. The nuclei were subsequently stained with DAPI (D9542, Sigma-Aldrich) for 5 min. Fluorescence images were acquired using a DMi8 fluorescence microscope (Leica Microsystems, Wetzlar, Germany) under identical imaging parameters. For quantitative analysis, three fields were randomly selected from each group, and the mean GSDMD fluorescence intensity was calculated using ImageJ.

Enzyme-Linked Immunosorbent Assay (ELISA)

ELISA kits from Wuhan Colorful Gene (Wuhan, China) were used to determine the levels of IL-1β and IL-18 in cell supernatants. The catalog numbers of the two kits were JYM0083Hu and JYM0092Hu, respectively. After cell treatment, the culture medium was collected and centrifuged to remove impurities. The clear supernatant was then carefully collected, and the assays were performed according to the manufacturer's instructions to determine the levels of the two inflammatory factors. Absorbance was measured using an iMark Microplate Absorbance Reader (168-1130, Bio-Rad, Hercules, CA, USA).

Flow Cytometry

An Annexin V-fluorescein isothiocyanate (FITC)/propidium iodide (PI) apoptosis detection kit (AP101, MULTI SCIENCES, Hangzhou, China) was used to assess overall cell death using a NovoCyte 3000 flow cytometer (Agilent/ACEA Biosciences, Santa Clara, CA, USA). Adherent cells were gently digested with EDTA-free trypsin (S310KJ, BasalMedia, Shanghai, China) to minimize cell damage and experimental variability, while suspended cells were directly collected by low-speed centrifugation. After digestion was terminated, approximately 1–5 × 10^5 cells were collected by centrifugation and washed twice with pre-cooled PBS. The cells were resuspended in 500 µL of 1× Binding Buffer, followed by the addition of 5 µL of Annexin V-FITC and 10 µL of PI to each sample. After gentle mixing, the cells were incubated at room temperature in the dark for 5 min and immediately analyzed by flow cytometry. Annexin V-FITC and PI fluorescence signals were detected using the FITC and PI channels, respectively. It should be noted that the proportion of positive cells measured in this assay was used only to reflect the overall level of cell death and could not, by itself, be considered a specific indicator of pyroptosis.

Statistical Analysis

Statistical analyses were performed using GraphPad Prism software (version 9.5, GraphPad Software, San Diego, CA, USA). The normality of continuous data was assessed using the Shapiro-Wilk test. Normally distributed data are presented as the mean ± standard deviation (SD). Comparisons between two groups were performed using an unpaired two-tailed Student's *t*-test. Comparisons among three or more groups were performed using one-way analysis of variance (ANOVA), followed by Tukey's multiple-comparison test when appropriate. For non-normally distributed data, the Mann-Whitney U test or Kruskal-Wallis test followed by Dunn's multiple-comparison test was used, as appropriate. All statistical tests were two-sided, and $p < 0.05$ was considered statistically significant.

Results

NEK7 Expression is Down-Regulated in NSCLC

We first analyzed the data using the UALCAN database. The transcriptional levels of *NEK7* were significantly lower in both lung adenocarcinoma and lung squamous cell carcinoma tissues than in normal lung tissues ($p < 0.05$) [Fig. 1a]. To further verify this finding at the cellular level, we then used qRT-PCR and Western blotting to examine NEK7 expression in normal bronchial epithelial HBE cells and several non-small cell lung cancer cell lines. Both assays consistently showed weaker NEK7 expression in the cancer cell lines than in HBE cells (all $p < 0.05$) [Fig. 1b–d]. These observations from tissue-derived datasets and cultured cells collectively support the down-regulation of NEK7 in NSCLC.

NEK7 Inhibits the Proliferation and Invasion of NSCLC Cells

NEK7 showed relatively low expression in the LUAD-derived A549 cells and LUSC-derived H1703 cells;

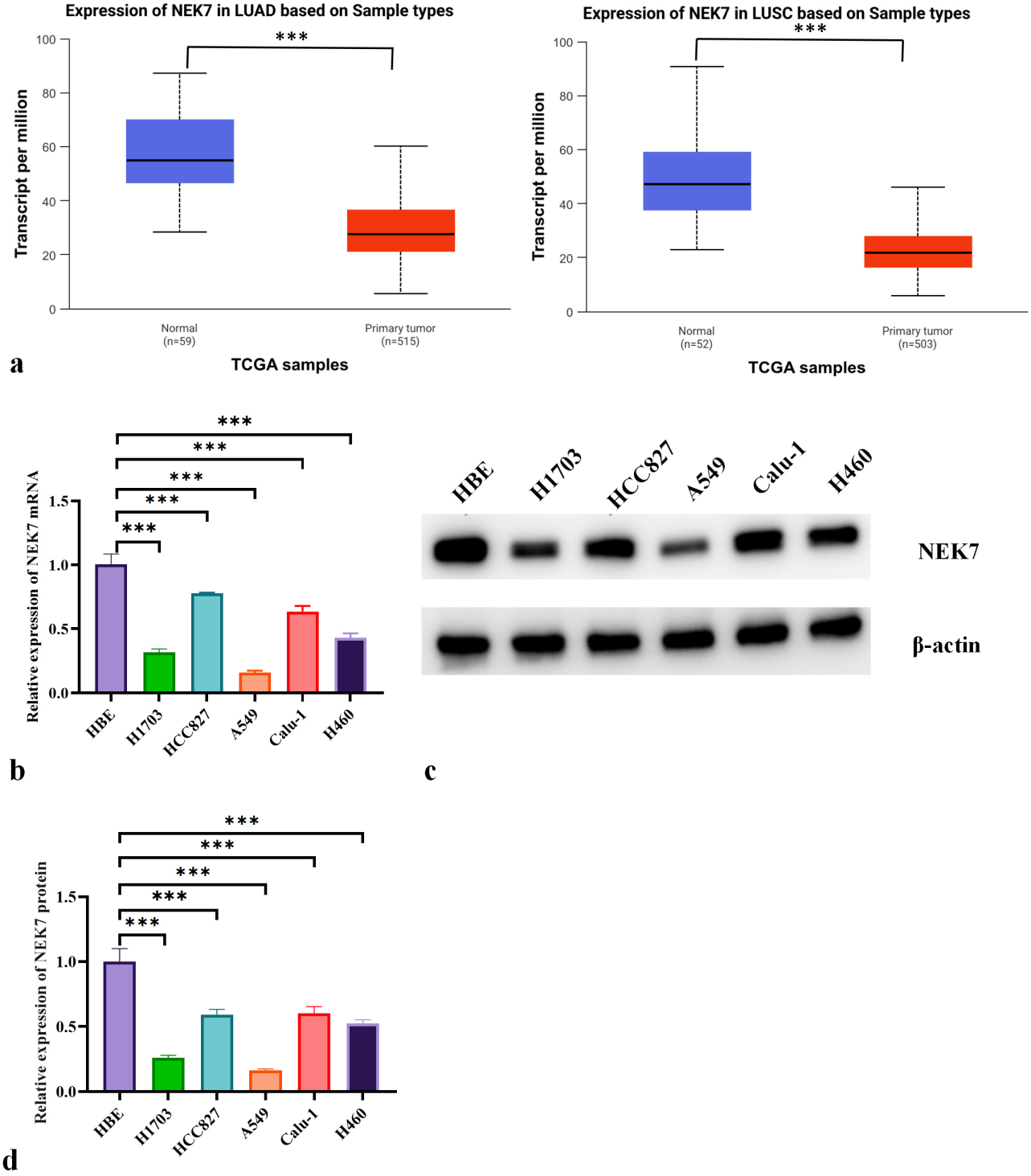

Fig. 1. NEK7 expression is down-regulated in NSCLC. (a) The UALCAN database was employed to assess *NEK7* expression in LUAD and LUSC samples. For LUAD, normal tissues, n = 59, and primary tumor tissues, n = 515; for LUSC, normal tissues, n = 52, and primary tumor tissues, n = 503. (b) The relative expression of *NEK7* mRNA in different NSCLC cell lines and HBE cell lines was detected by qRT-PCR. (c,d) The relative expression of NEK7 protein in different NSCLC cell lines and normal lung bronchial epithelial cell lines was detected by WB. For the cell-based experiments in (b–d), n = 6; ***$p < 0.001$. NEK7, NIMA-related kinase 7; NSCLC, non-small cell lung cancer; LUAD, lung adenocarcinoma; LUSC, lung squamous cell carcinoma; qRT-PCR, quantitative real-time polymerase chain reaction; WB, western blotting.

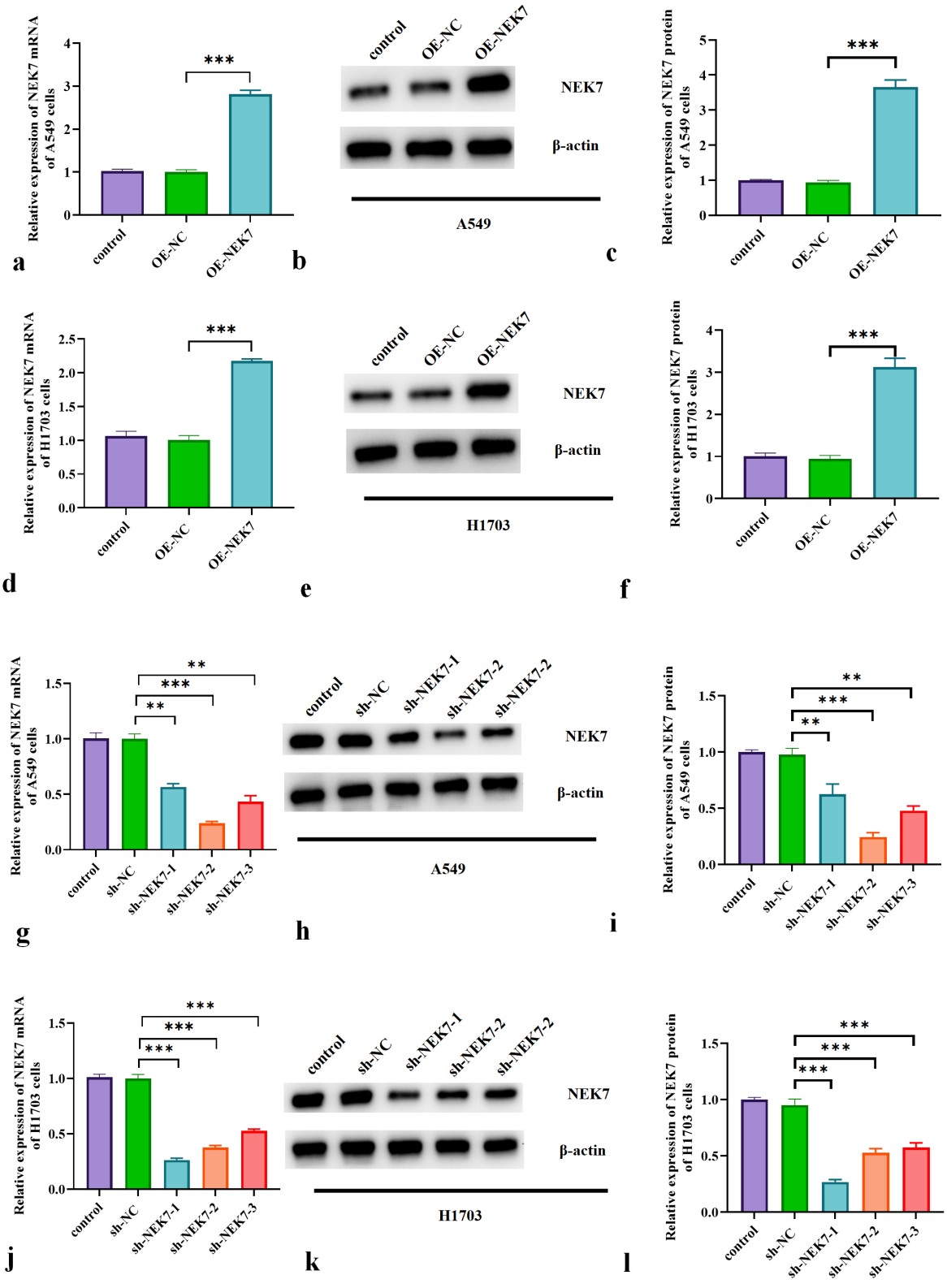

Fig. 2. Transfection efficiency was verified using qRT-PCR and WB. (a–c) qRT-PCR and WB analyses assessed the efficiency of *NEK7* gene overexpression in the A549 cell line. (d–f) qRT-PCR and WB analyses assessed the efficiency of *NEK7* gene overexpression in the H1703 cell line. (g–i) qRT-PCR and WB analyses assessed the efficiency of *NEK7* gene knockdown in the A549 cell line. (j–l) qRT-PCR and WB analyses assessed the efficiency of *NEK7* gene knockdown in the H1703 cell line. n = 6; $^{**}p < 0.01$, $^{***}p < 0.001$.

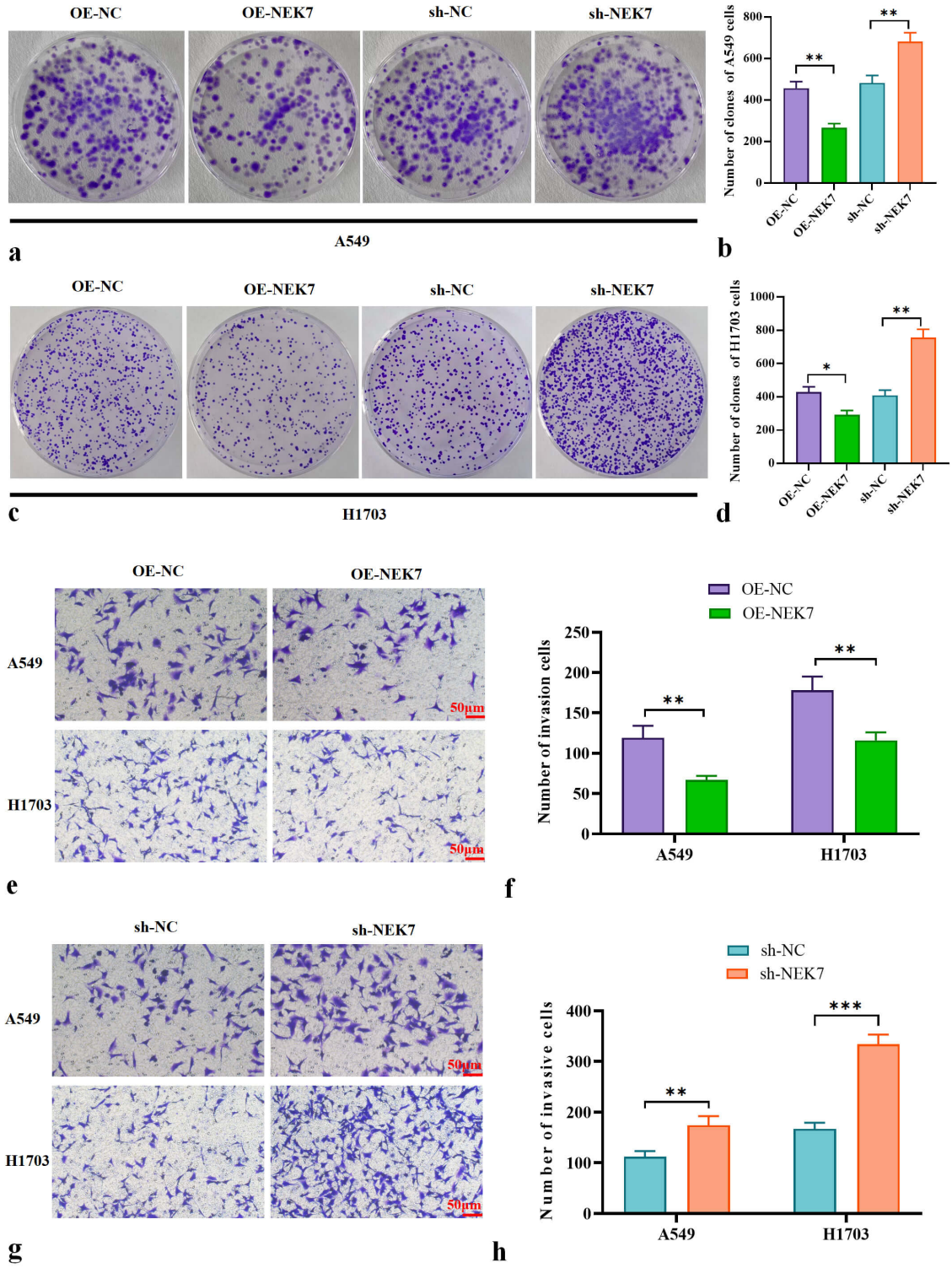

Fig. 3. NEK7 inhibits the proliferation and invasion of NSCLC cells. (a–d) The proliferative ability was tested by a colony formation experiment. (e–h) The invasion ability was detected by Transwell experiments. n = 6; *$p < 0.05$, **$p < 0.01$, ***$p < 0.001$. NSCLC, non-small cell lung cancer.

therefore, these two cell lines were chosen for subsequent experiments. NEK7 gain- and loss-of-function models were then established, and transfection efficiency was confirmed. As illustrated in Fig. 2a–l, OE-NEK7 treatment significantly increased NEK7 expression relative to OE-NC, whereas all three shRNA constructs reduced NEK7 expres-

sion in both A549 and H1703 cells (all $p < 0.05$). Among the three knockdown constructs, sh-NEK7-2 achieved the greatest reduction in A549 cells and was therefore used in the following assays. In H1703 cells, sh-NEK7-1 showed the strongest silencing effect and was selected for subsequent analyses [Fig. 2g–l]. Colony formation assays were used to examine the growth potential of cells after manipulating NEK7 expression. After NEK7 knockdown, the colony-forming ability of both A549 and H1703 lung cancer cells was significantly increased. In contrast, NEK7 overexpression exerted the opposite effect and markedly suppressed clonogenic growth, with statistically significant differences among the groups ($p < 0.05$) [Fig. 3a–d]. The Transwell invasion assay yielded consistent results. Compared with the negative control group, silencing NEK7 significantly increased the number of tumor cells that penetrated the Matrigel barrier ($p < 0.05$) [Fig. 3e–h]. Conversely, increasing NEK7 expression effectively reduced the number of cells invading through the barrier ($p < 0.05$). Taken together, these findings indicate that NEK7 suppresses the proliferation and invasion of non-small cell lung cancer cells, whereas reduced NEK7 expression markedly enhances the malignant invasive behavior of lung cancer cells.

NEK7 Affects Pyroptosis-Related Changes in NSCLC Cells

Changes in GSDMD fluorescence were examined after altering NEK7 expression. Immunofluorescence analysis revealed stronger GSDMD signals following NEK7 overexpression, whereas NEK7 silencing exerted the opposite effect in both A549 and H1703 cells (both $p < 0.01$) [Fig. 4a–c].

NEK7 is Associated With NLRP3-Related Pyroptosis-Related Changes in NSCLC Cells

Western blot analysis was used to assess NLRP3, ASC, and Caspase-1 in A549 and H1703 cells following manipulation of NEK7 expression. Increasing NEK7 expression increased the expression levels of all three proteins, whereas NEK7 silencing produced the opposite effect (all $p < 0.01$) [Fig. 5a–d]. The concentrations of IL-1β and IL-18 in culture supernatants were further measured using ELISA. In A549 cells, both cytokines were higher in the OE-NEK7 group than in the OE-NC group (both $p < 0.01$), while NEK7 knockdown reduced their levels relative to sh-NC (both $p < 0.01$). Comparable changes were also observed in H1703 cells [Fig. 5e–h].

NLRP3 Inhibition Partially Reverses the Effects of NEK7 Overexpression on NSCLC Cells

To examine the possible involvement of NLRP3 signaling in the cellular effects of NEK7 overexpression in NSCLC cells, A549 and H1703 cells were divided into three groups: OE-NC, OE-NEK7, and OE-NEK7+MCC950. As presented in Fig. 6a–d, addition of MCC950 to NEK7-overexpressing cells decreased the proportion of Annexin V-FITC/PI-positive cells relative to NEK7 overexpression alone ($p < 0.05$). Colony formation analysis further showed that MCC950 treatment restored clonogenic growth that had been suppressed by NEK7 overexpression ($p < 0.05$) [Fig. 6e,f]. A similar response was observed in the Transwell experiment, where MCC950 increased the invasive cell count following NEK7 overexpression ($p < 0.05$) [Fig. 6g,h]. Collectively, these pharmacological findings suggest that MCC950 attenuates the cellular changes associated with NEK7 overexpression, providing supportive evidence for the possible involvement of NLRP3-related signaling.

Discussion

Our data revealed reduced NEK7 expression in NSCLC cells, consistent with the expression pattern observed in LUAD and LUSC in the UALCAN dataset. The cell functional assays confirmed that increasing NEK7 expression effectively suppressed the clonogenic growth and invasive ability of A549 and H1703 cells. In contrast, NEK7 knockdown markedly enhanced the proliferative and invasive capacities of lung cancer cells. Notably, these findings are completely different from those reported in hepatocellular, gastric, and pancreatic cancers, where previous studies have shown that NEK7 promotes tumor progression [21,22,23]. These opposite effects suggest that the regulatory role of NEK7 in tumors may vary depending on tumor type and cellular microenvironment.

Pyroptotic signaling has now been recognized as an important mechanism involved in tumor progression [24]. Our experimental results showed that increased NEK7 expression markedly enhanced intracellular GSDMD fluorescence intensity, increased the expression levels of NLRP3 pathway-related proteins, and significantly elevated the secretion of the inflammatory factors IL-1β and IL-18. In contrast, NEK7 knockdown markedly reduced all of these pyroptosis-related indicators, showing an opposite pattern of change. Together, these results indicate that alterations in NEK7 expression are associated with changes in the NLRP3-related pyroptotic machinery in NSCLC cells [25,26,27]. Previous studies have shown that NEK7 can cooperate with NLRP3 during inflammasome assembly and activation [28,29,30]. Nevertheless, the present experiments did not directly assess NEK7–NLRP3 binding using co-immunoprecipitation or other interaction-based approaches. Therefore, our results support the involvement of the NLRP3-related pathway but cannot establish a direct physical or regulatory relationship between these two proteins.

The role of NLRP3 was further explored pharmacologically using MCC950 in cells with elevated NEK7 expression [31]. Blocking NLRP3 reduced NEK7-associated

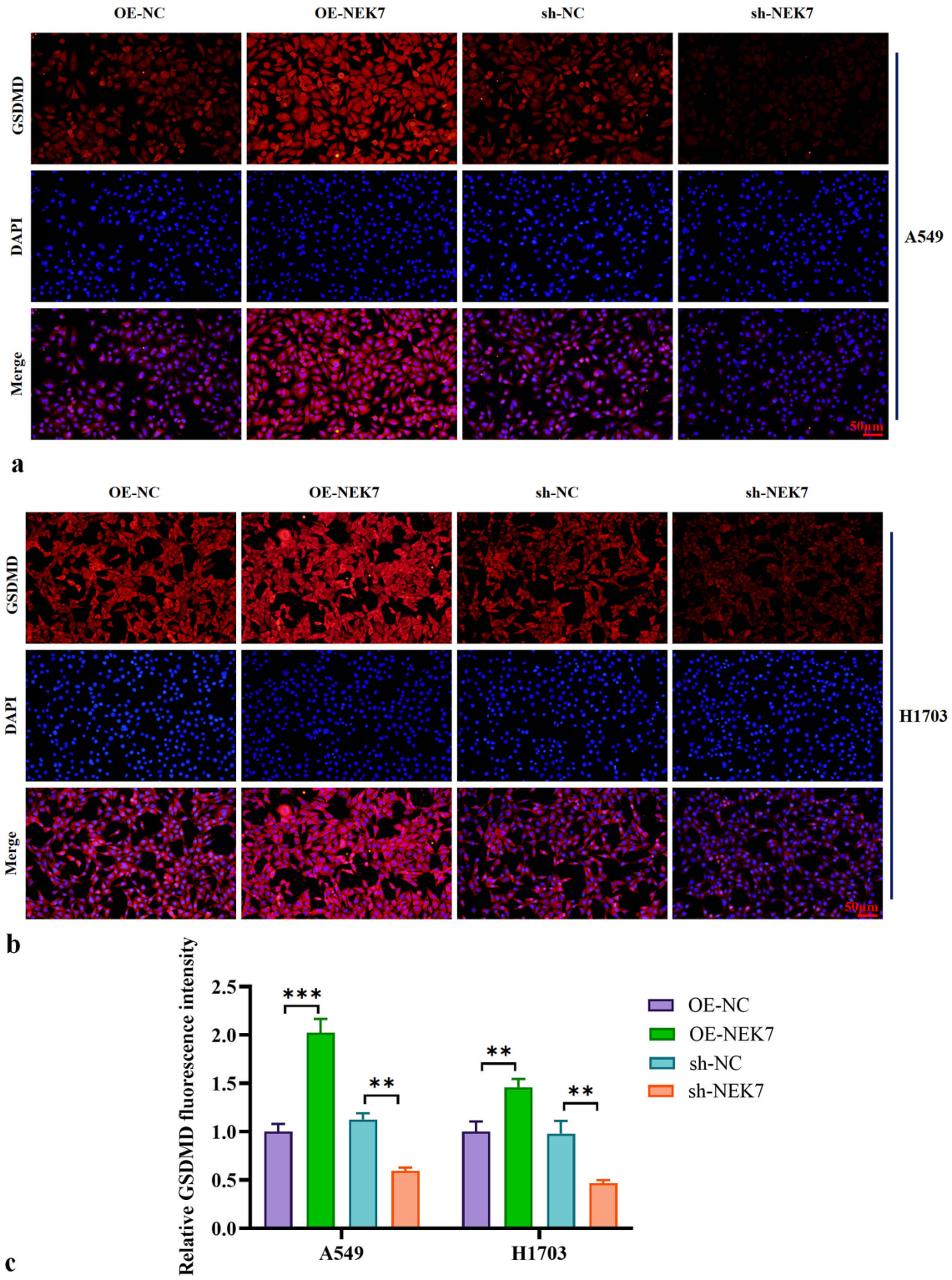

Fig. 4. NEK7 affects pyroptosis-related changes in NSCLC cells. (a–c) Immunofluorescence staining analysis of GSDMD fluorescence intensity after NEK7 overexpression or knockdown in A549 and H1703 cells. n = 6; $^{**}p < 0.01$, $^{***}p < 0.001$. GSDMD, Gasdermin D.

cell death and restored part of the clonogenic and invasive capacity that had been lost after NEK7 overexpression. This response suggests that NLRP3-related signaling may be involved in the cellular changes associated with NEK7 overexpression. However, Annexin V-FITC/PI positivity should be interpreted as an overall indicator of cell death

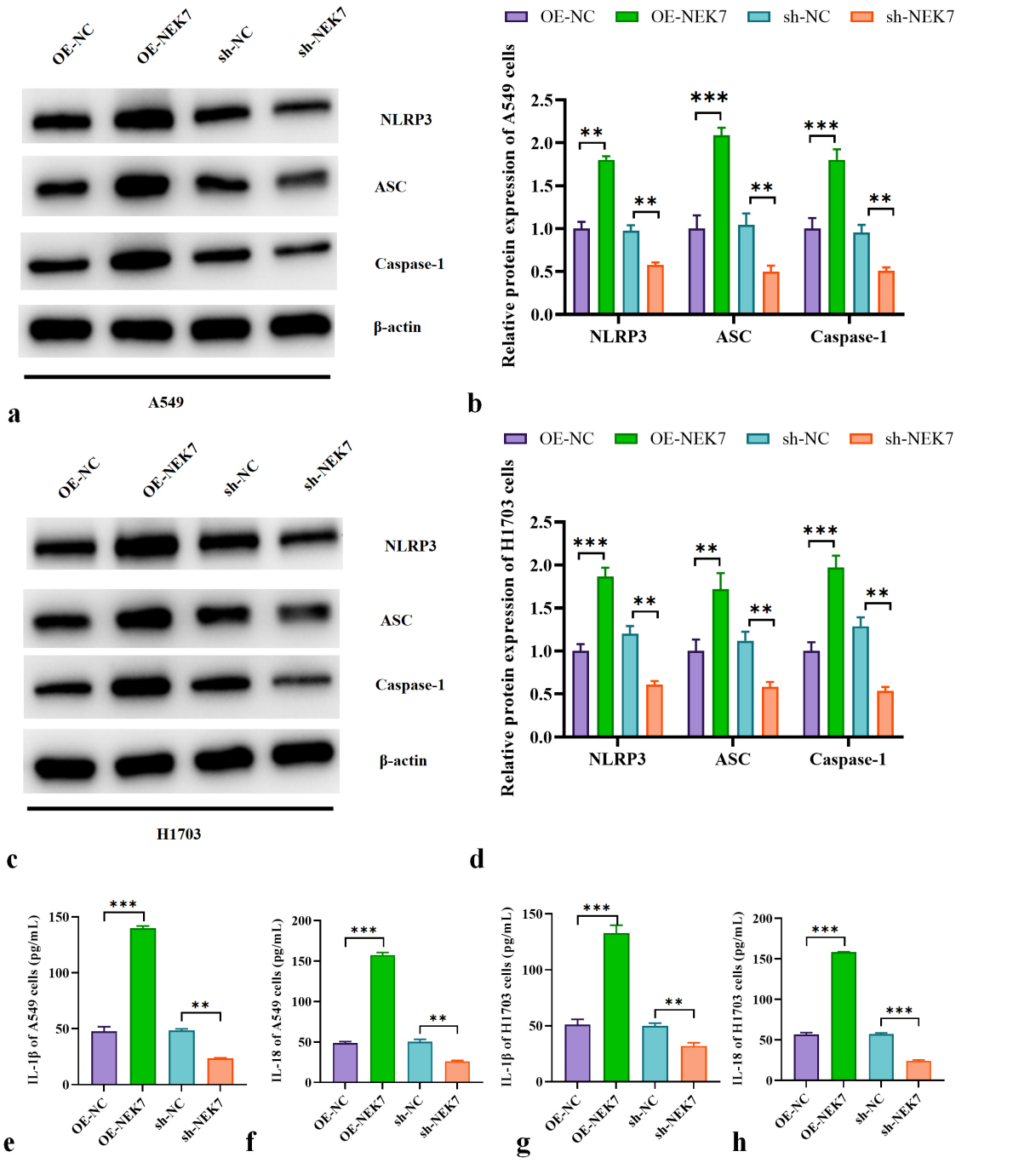

Fig. 5. NEK7 affects NLRP3 inflammasome-associated pyroptosis-related changes in NSCLC cells. (a–d) WB analysis of pyroptosis-related proteins in A549 and H1703 cells. (e–h) The levels of IL-1β and IL-18 were quantified by ELISA in A549 and H1703 cells. n = 6; $^{**}p < 0.01$, $^{***}p < 0.001$. NLRP3, NOD-like receptor family pyrin domain-containing 3; IL, interleukin; ELISA, Enzyme-Linked Immunosorbent Assay.

rather than a pyroptosis-specific endpoint, because a similar staining pattern can also occur during late apoptosis. In addition, NEK7 participates in cell-cycle control. Thus, the growth-inhibitory effect observed following increased NEK7 expression may reflect both NLRP3-associated pyroptotic events and NLRP3-independent mechanisms, including alterations in cell-cycle regulation [32,33].

Several limitations related to the mechanistic interpretation of our findings should be acknowledged, particularly regarding the evidence for NEK7–NLRP3 regulation, pyroptosis assessment, and pharmacological inhibition. First, the evidence supporting pyroptosis remains limited because GSDMD-N, cleaved Caspase-1, and indicators of membrane rupture, such as LDH release, were not examined.

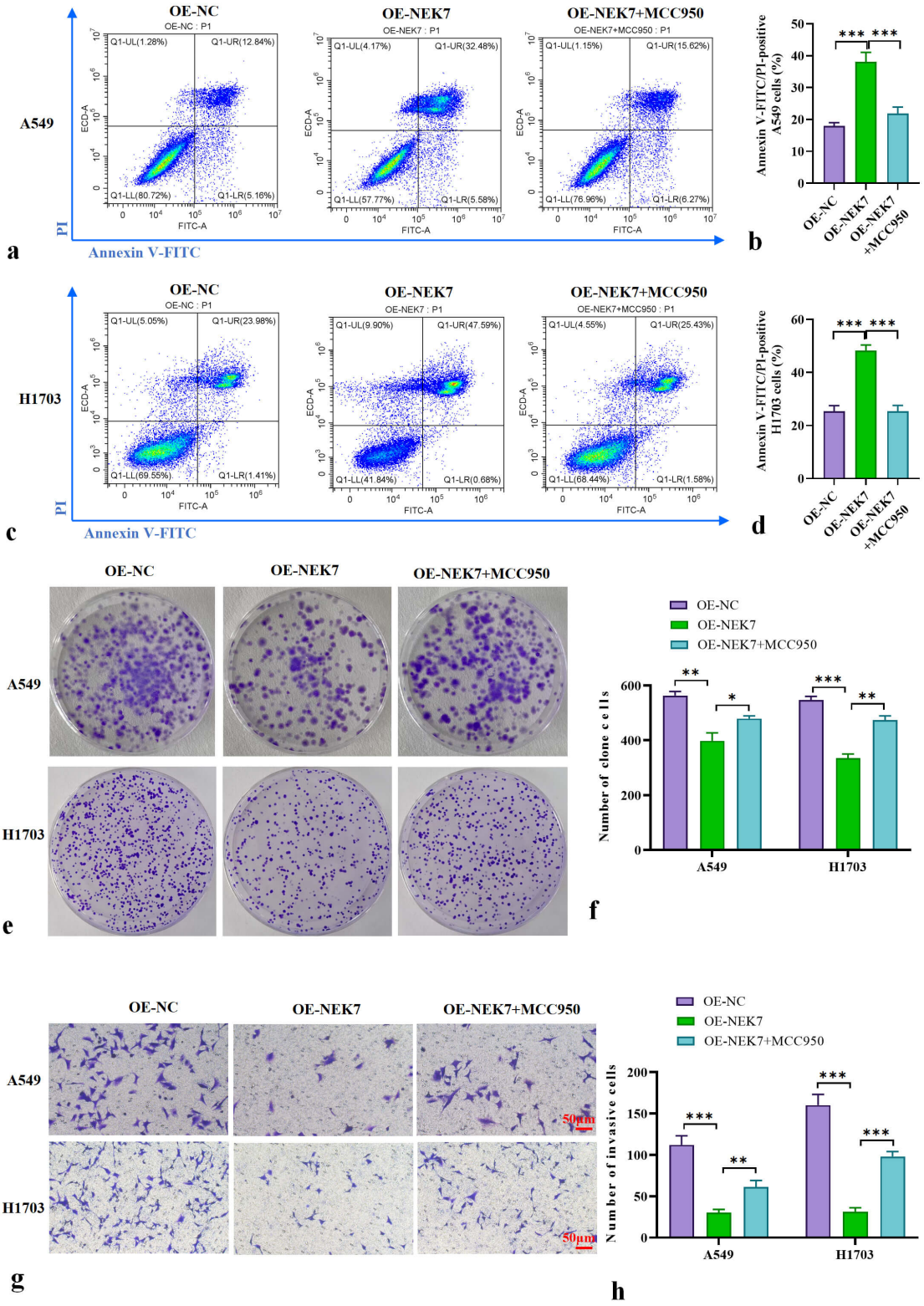

Fig. 6. MCC950 partially reverses the effects associated with NEK7 overexpression in NSCLC cells. (a–d) Cell death was assessed by Annexin V-FITC/PI flow cytometry in A549 and H1703 cells. (e,f) The proliferative capacity was tested by a colony formation assay in A549 and H1703 cells. (g,h) The invasion ability was detected by a Transwell assay in A549 and H1703 cells. n = 6; *$p < 0.05$, **$p < 0.01$, ***$p < 0.001$. FITC, fluorescein isothiocyanate; PI, Propidium iodide.

Apoptosis-specific markers such as cleaved caspase-3 were also not assessed; therefore, the involvement of other forms of cell death cannot be completely excluded. Second, a relatively high baseline Annexin V-FITC/PI-positive rate was observed in the OE-NC group, particularly in H1703 cells. This may be partly attributable to cellular stress induced by transfection or differences in the sensitivity of different cell lines to the transfection procedure. Although the OE-NC and OE-NEK7 groups were subjected to the same transfection and culture conditions, this background level of cell death should still be considered when interpreting the flow cytometry results. Third, the MCC950 rescue experiment did not include an MCC950-alone group or a corresponding vehicle control, making it difficult to completely exclude independent effects of MCC950 or its vehicle. In addition, genetic validation by NLRP3 knockdown or knockout was not performed; therefore, the MCC950 experiment provides supportive rather than definitive evidence for the involvement of NLRP3. Fourth, the direct protein–protein interaction between NEK7 and NLRP3 was not verified by Co-immunoprecipitation or other protein-interaction assays, and the upstream mechanisms underlying NEK7 down-regulation, as well as the possible involvement of other signaling pathways, remain unclear. Finally, the present findings were mainly obtained from *in vitro* experiments and require further validation in animal models and clinical samples. Future studies incorporating key pyroptosis markers, membrane rupture assays, appropriate controls, protein–protein interaction assays, cell-cycle analysis, and *in vivo* experiments may further clarify the role of NEK7 in NSCLC. In addition, the present study did not examine the associations between NEK7 expression and clinicopathological characteristics or patient prognosis. Therefore, the clinical significance of NEK7 in NSCLC cannot be determined based on the current data.

Conclusions

Our findings show that NEK7 is downregulated in NSCLC and that increased NEK7 expression is associated with reduced clonogenic growth and invasive capacity in A549 and H1703 cells. NEK7 overexpression was also accompanied by changes in NLRP3-associated pyroptosis markers, while MCC950 partially attenuated the cellular changes associated with NEK7 overexpression, suggesting the possible involvement of NLRP3-related signaling. These results suggest that increased NEK7 expression is associated with less aggressive cellular behavior in NSCLC models, although its clinical relevance and underlying mechanisms require further investigation.

Availability of Data and Materials

The datasets used or analyzed during this study are available from the corresponding author on reasonable request.

Author Contributions

QYL designed the study and contributed to conceptualization and methodology. QYL and SFY conducted data collection, investigation, data curation, and validation. XQC performed formal analysis, contributed to methodology development, and conducted visualization. LJZ contributed to the study design and methodology, supervised the study, secured funding, and contributed to project administration. QYL drafted the original manuscript. All authors contributed to the critical revision of the manuscript for important intellectual content. All authors have read and approved the final manuscript. All authors have participated sufficiently in the work to take public responsibility for appropriate portions of the content and agreed to be accountable for all aspects of the work in ensuring that questions related to its accuracy or integrity.

Ethics Approval and Consent to Participate

Not applicable.

Acknowledgment

Not applicable.

Funding

This study was supported by the Medical and Health Research Project of Zhejiang Province (2024KY400), Beijing Science And Technology Innovation Medical Development Foundation (KC2023-JX-0186-PQ011), and Wenzhou Municipal Science and Technology Project (YC20260914).

Conflict of Interest

The authors declare no conflict of interest.

References

[1] Schabath MB, Cote ML. Cancer Progress and Priorities: Lung Cancer. Cancer Epidemiology, Biomarkers & Prevention: a Publication of the American Association for Cancer Research, Cosponsored by the American Society of Preventive Oncology. 2019; 28: 1563–1579. https://doi.org/10.1158/1055-9965.EPI-19-0221

[2] Relli V, Trerotola M, Guerra E, Alberti S. Abandoning the Notion of Non-Small Cell Lung Cancer. Trends in Molecular Medicine. 2019; 25: 585–594. https://doi.org/10.1016/j.molmed.2019.04.012

[3] Zhang J, Mou Y, Li H, Shen H, Song J, Li Q. LINC00638 promotes the progression of non-small cell lung cancer by regulating the miR-541-3p/IRS1/PI3K/Akt axis. Heliyon. 2023; 9: e16999. https://doi.org/10.1016/j.heliyon.2023.e16999

[4] Imyanitov EN, Iyevleva AG, Levchenko EV. Molecular testing and targeted therapy for non-small cell lung cancer: Current status and perspectives. Critical Reviews in Oncology/hematology. 2021; 157: 103194. https://doi.org/10.1016/j.critrevonc.2020.103194

[5] Nagano T, Tachihara M, Nishimura Y. Molecular Mechanisms and Targeted Therapies Including Immunotherapy for Non-Small Cell Lung Cancer. Current Cancer Drug Targets. 2019; 19: 595–630. https://doi.org/10.2174/1568009619666181210114559

[6] Zhou S, Xu Y, Tu J, Zhang M. Inhibiting NLRP3/Caspase-1/GSDMD-Mediated Pyroptosis: A New Role of GADD45B's Role in Hypertriglyceridemia-Induced Acute Pancreatitis. Discovery Medicine. 2025; 37: 1105–116. https://doi.org/10.24976/Discov.Med.202537197.98

[7] Ketelut-Carneiro N, Fitzgerald KA. Apoptosis, Pyroptosis, and Necroptosis-Oh My! The Many Ways a Cell Can Die. Journal of Molecular Biology. 2022; 434: 167378. https://doi.org/10.1016/j.jmb.2021.167378

[8] Fang Y, Tian S, Pan Y, Li W, Wang Q, Tang Y, et al. Pyroptosis: A new frontier in cancer. Biomedicine & Pharmacotherapy = Biomedecine & Pharmacotherapie. 2020; 121: 109595. https://doi.org/10.1016/j.biopha.2019.109595

[9] Li S, Sun Y, Song M, Song Y, Fang Y, Zhang Q, et al. NLRP3/caspase-1/GSDMD-mediated pyroptosis exerts a crucial role in astrocyte pathological injury in mouse model of depression. JCI Insight. 2021; 6: e146852. https://doi.org/10.1172/jci.insight.146852

[10] Coll RC, Schroder K, Pelegrín P. NLRP3 and pyroptosis blockers for treating inflammatory diseases. Trends in Pharmacological Sciences. 2022; 43: 653–668. https://doi.org/10.1016/j.tips.2022.04.003

[11] Sharma BR, Kanneganti TD. NLRP3 inflammasome in cancer and metabolic diseases. Nature Immunology. 2021; 22: 550–559. https://doi.org/10.1038/s41590-021-00886-5

[12] Huang H, Weng Y, Tian W, Lin X, Chen J, Luo L. Molecular mechanisms of pyroptosis and its role in anti-tumor immunity. International Journal of Biological Sciences. 2023; 19: 4166–4180. https://doi.org/10.7150/ijbs.86855

[13] Yan H, Luo B, Wu X, Guan F, Yu X, Zhao L, et al. Cisplatin Induces Pyroptosis via Activation of MEG3/NLRP3/caspase-1/GSDMD Pathway in Triple-Negative Breast Cancer. International Journal of Biological Sciences. 2021; 17: 2606–2621. https://doi.org/10.7150/ijbs.60292

[14] Guan X, Liu R, Wang B, Xiong R, Cui L, Liao Y, et al. Inhibition of HDAC2 sensitises antitumour therapy by promoting NLRP3/GSDMD-mediated pyroptosis in colorectal cancer. Clinical and Translational Medicine. 2024; 14: e1692. https://doi.org/10.1002/ctm2.1692

[15] Dahiya R, Sutariya VB, Gupta SV, Pant K, Ali H, Alhadrawi M, et al. Harnessing pyroptosis for lung cancer therapy: The impact of NLRP3 inflammasome activation. Pathology, Research and Practice. 2024; 260: 155444. https://doi.org/10.1016/j.prp.2024.155444

[16] Wang J, Chen S, Liu M, Zhang M, Jia X. NEK7: a new target for the treatment of multiple tumors and chronic inflammatory diseases. Inflammopharmacology. 2022; 30: 1179–1187. https://doi.org/10.1007/s10787-022-01026-7

[17] Sharif H, Wang L, Wang WL, Magupalli VG, Andreeva L, Qiao Q, et al. Structural mechanism for NEK7-licensed activation of NLRP3 inflammasome. Nature. 2019; 570: 338–343. https://doi.org/10.1038/s41586-019-1295-z

[18] Chen X, Liu G, Yuan Y, Wu G, Wang S, Yuan L. NEK7 interacts with NLRP3 to modulate the pyroptosis in inflammatory bowel disease via NF-κB signaling. Cell Death & Disease. 2019; 10: 906. https://doi.org/10.1038/s41419-019-2157-1

[19] Chandrashekar DS, Karthikeyan SK, Korla PK, Patel H, Shovon AR, Athar M, et al. UALCAN: An update to the integrated cancer data analysis platform. Neoplasia (New York, N.Y.). 2022; 25: 18–27. https://doi.org/10.1016/j.neo.2022.01.001

[20] Zhao Z, Chen X, Feng Y, Lei Y, Deng X, Lin R, et al. Identification of the important role of CA9 in immune infiltration and prognosis in cervical cancer. Future Science OA. 2025; 11: 2532314. https://doi.org/10.1080/20565623.2025.2532314

[21] Yan Z, Qu J, Li Z, Yi J, Su Y, Lin Q, et al. NEK7 Promotes Pancreatic Cancer Progression And Its Expression Is Correlated With Poor Prognosis. Frontiers in Oncology. 2021; 11: 705797. https://doi.org/10.3389/fonc.2021.705797

[22] Zhou L, Wang Z, Xu X, Wan Y, Qu K, Fan H, et al. Nek7 is overexpressed in hepatocellular carcinoma and promotes hepatocellular carcinoma cell proliferation in vitro and in vivo. Oncotarget. 2016; 7: 18620–18630. https://doi.org/10.18632/oncotarget.7620

[23] Li YK, Zhu XR, Zhan Y, Yuan WZ, Jin WL. NEK7 promotes gastric cancer progression as a cell proliferation regulator. Cancer Cell International. 2021; 21: 438. https://doi.org/10.1186/s12935-021-02148-8

[24] Wei X, Xie F, Zhou X, Wu Y, Yan H, Liu T, et al. Role of pyroptosis in inflammation and cancer. Cellular & Molecular Immunology. 2022; 19: 971–992. https://doi.org/10.1038/s41423-022-00905-x

[25] Yao F, Jin Z, Zheng Z, Lv X, Ren L, Yang J, et al. HDAC11 promotes both NLRP3/caspase-1/GSDMD and caspase-3/GSDME pathways causing pyroptosis via ERG in vascular endothelial cells. Cell Death Discovery. 2022; 8: 112. https://doi.org/10.1038/s41420-022-00906-9

[26] Li LR, Chen L, Sun ZJ. Igniting hope: Harnessing NLRP3 inflammasome-GSDMD-mediated pyroptosis for cancer immunotherapy. Life Sciences. 2024; 354: 122951. https://doi.org/10.1016/j.lfs.2024.122951

[27] Lin TY, Tsai MC, Tu W, Yeh HC, Wang SC, Huang SP, et al. Role of the NLRP3 Inflammasome: Insights Into Cancer Hallmarks. Frontiers in Immunology. 2021; 11: 610492. https://doi.org/10.3389/fimmu.2020.610492

[28] Li Q, Feng H, Wang H, Wang Y, Mou W, Xu G, et al. Licochalcone B specifically inhibits the NLRP3 inflammasome by disrupting NEK7-NLRP3 interaction. EMBO Reports. 2022; 23: e53499. https://doi.org/10.15252/embr.202153499

[29] Shi H, Wang Y, Li X, Zhan X, Tang M, Fina M, et al. NLRP3 activation and mitosis are mutually exclusive events coordinated by NEK7, a new inflammasome component. Nature Immunology. 2016; 17: 250–258. https://doi.org/10.1038/ni.3333

[30] Fu J, Wu H. Structural Mechanisms of NLRP3 Inflammasome Assembly and Activation. Annual Review of Immunology. 2023; 41: 301–316. https://doi.org/10.1146/annurev-immunol-081022-021207

[31] Perera AP, Fernando R, Shinde T, Gundamaraju R, Southam B, Sohal SS, et al. MCC950, a specific small molecule inhibitor of NLRP3 inflammasome attenuates colonic inflammation in spontaneous colitis mice. Scientific Reports. 2018; 8: 8618. https://doi.org/10.1038/s41598-018-26775-w

[32] Feng SH, Zhao B, Zhan X, Li RH, Yang Q, Wang SM, et al. Quercetin-induced pyroptosis in colon cancer through NEK7-mediated NLRP3 inflammasome-GSDMD signaling pathway activation. American Journal of Cancer Research. 2024; 14: 934–958. https://doi.org/10.62347/MKAN3550

[33] Swanson KV, Deng M, Ting JPY. The NLRP3 inflammasome: molecular activation and regulation to therapeutics. Nature Reviews. Immunology. 2019; 19: 477–489. https://doi.org/10.1038/s41577-019-0165-0